J Intell Robot Syst (2014) 74:945–963
DOI 10.1007/s10846-013-9856-0

On the Complete Coverage Path Planning for Mobile Robots

Ping-Min Hsu · Chun-Liang Lin · Meng-Yao Yang

Received: 5 July 2012 / Accepted: 6 June 2013 / Published online: 7 July 2013

Abstract This paper presents a generalized complete coverage path planning (CCPP) algorithm and its implementation for a mobile robot. The proposed planner contains two concerns: 1) low working time or low energy consumption, and 2) high human safety. For the first concern, we design the optimal path by incorporating two factors: time and energy costs. Describing the working time and energy in terms of a turning parameter simplifies the optimal path design either for minimizing the time or energy cost. For obstacle avoidance in the CCPP, fixed or moving objects are avoided by proposing a field method describing the effects of factors such as working dangerousness and difficulty on the current robot navigation. The human safety is simultaneously guaranteed by this method. Furthermore, a backstepping controller considering constraints imposed on the control input is established to track the optimal route. An implementation of the proposed CCPP for the experimentally mobile robot equipped with this controller is presented; the verification results demonstrate significant performance and practicality of the proposed strategy.

Keywords Backstepping control · Complete coverage path planning · Human safety · Optimization

Mathematics Subject Classification (2010) 68T40

P.-M. Hsu · C.-L. Lin (✉) · M.-Y. Yang
Department of Electrical Engineering,
National Chung Hsing University,
Taichung, Taiwan 402, Republic of China
e-mail: chunlin@dragon.nchu.edu.tw

1 Introduction

Nowadays, consumers pay a considerable attention to service robots for possible use in human daily life. The theoretical-based researches related to these robots, such as the mowing or cleaning robot, have been widely addressed in the literature in the past decade. One of them is the study of the robot path planning termed complete coverage path planning (CCPP), which means that the whole workspace must be swept out. The term "complete coverage" implies that integrating the subarea the robot passed by generates the same working field. Choset [1] surveyed past CCPP researches while many of them were developed within the workspace which was localized beforehand by a geometric structure, namely cellular decomposition. To enhance the localization accuracy, Zu et al. [2] proposed a localization method combined with a neural network. Ensured the acceptable accuracy, Lee et al. [3] investigated the

on-line path planning for the cleaning robots by the cellular decomposition describing the environment of workspace in terms of grid. Two conventional tools including genetic algorithm and neural network are implemented to design the CCPP. Yang et al. [4] proposed the neural network based approach for the CCPP including the obstacle avoidance in the non-stationary environments of the cleaning robots. Luo et al. [5] solved the CCPP problem involving obstacle avoidance by using a biologically inspired neural network. Qiu et al. [6] developed the path planning method by combining neural network, rolling path planning, and heuristic searching approaches; they adopted the neural network to characterize the environmental effect on the CCPP. Qiu et al. [7] established the path planning method integrating rolling windows and biologically inspired neural networks based on the object avoidance concern. Luo et al. [8] developed the CCPP for multiple cleaning robots by a biologically inspired neural network which computes the collision-free robot routes within the workspace. Each cleaner treats others as the moving obstacles and avoids them. Additionally, Sipahioglu et al. [9] applied capacitated arc routing approaches to develop the multi-robot sensor-based CCPP under the working energy constraint.

Several published literature proposed the optimal CCPP based on the optimization techniques, genetic algorithms. Yao [10] proposed the CCPP incorporating a modified sweeping line strategy and geometric algorithm which minimizes the extra relocation moves. Jimenez et al. [11] designed the optimal path by genetic algorithms. Moreover, Wang et al. [12] and Zhang et al. [13] constructed the CCPP according to sensors' information. Liu et al. [14] constructed the CCPP combined with the random path planning for the local route design. Vidal et al. [15] established the path planner including avoidance of the unexpected obstacles to create a priori map. Liu et al. [16] studied the on-line path planning featuring the moving object avoidance. Mao, et al. [17] dealt with the combined problem containing the template-based and the heuristic coverage path planning. Opposing to design the CCPP within the localized workspace in [2–17], other published works pay attention to the CCPP in unknown environments. Luo et al. [18] designed a neural network-based approach for the CCPP in the unknown environment. Oh et al. [19] established a solution of complete coverage navigation for the cleaning robots within the unknown workspace. Garcia et al. [20] used sensor data to establish CCPP in the unstructured environment. After the construction of the path planning, global positioning system (GPS) can be utilized to locate the waypoints (see [21]).

As for the path tracking, the mobile robots require a tracking controller to fultill the navigation task. For example, Chwa et al. [22], Park et al. [23], and Yavuz et al. [24] proposed the backstepping, adaptive, and fuzzy controllers for this task.

However, previous works [3–5, 9, 10, 12–15, 17, 18, 20, 21] and [6–8, 11, 16, 19] on the CCPP didn't cover the moving obstacle avoidance and the optimization of time or energy consumption, respectively. Moreover, the concern of human safety in either CCPP or robot navigation was not received much attention in the previous approaches. This motivates our pervious works [25, 26]. Despite the lawn mower design was initially presented in [25], the obstacle avoidance was not considered. In [26], the drawback was improved in the CCPP ensuring obstacle avoidance and human safety. However, in applications of this planner, the appearance of tracking errors in the robotic navigation may reduce the previously ensured human safety. It is possible that humans may be threatened by robot motion while the robot works away from its predesigned path in practice. Motivated by this fact, we propose an improved CCPP while considering the tracking errors of the robotic navigation.

The proposed CCPP consists of two parts—an off-line planner featuring optimal working efficiency and the on-line operation guaranteeing the human safety in the robot navigation. The off-line manner comprises the functions of minimal time mode, minimal energy mode, and mixed mode, as well as the optimal solution of CCPP problem. Furthermore, the on-line planner is designed to guarantee the obstacle avoidance and the human safety in applications of autonomous robots. As for the path tracking control, a backstepping controller is developed for the mobile robot described by a kinetic model with holonomic constraints which were ignored in [26]; it enables

the robot to track the optimal path. Feasibility of the proposed design has been well validated via real-world experiments.

This paper reveals three contributions: 1) the general solution of CCPP focusing on either the cost minimization of the working time or energy; 2) consideration of the tracking errors in the CCPP; and 3) the guarantee of the human safety in the robot navigation. This helps to improve practicability of the CCPP.

2 Problem Statements

The appropriate path proposition for the mowing or cleaning robots is a critical process which must be accomplished by the CCPP strategy before the robot implementations. In real-world applications, one may choose an arbitrary CCPP path without any optimal sense; however, optimization of the working time and energy for cost conservation is quite important for the CCPP due to performance concern. In practice, the CCPP requires the fixed or moving obstacle avoidance and simultaneously ensures the human safety in the robot navigation. The term "human safety" means that the robot would be far away from the humans within the workspace. Therefore, the goal here is to propose a CCPP focusing on the cost minimization and human safety in the robot navigation.

3 Complete Coverage Path Planning

The CCPP containing the minimum time, minimum energy, and mixed modes is proposed to achieve satisfactory performance based on three concerns: 1) the minimum time mode refers to the least time cost under the same energy consumption of the robot task; 2) the minimum energy mode refers to the least energy consumption under the same time consumption of completing the task; and 3) the mixed mode blends the two modes depicted.

Tracking the robot routes with sharp curves brings more difficulties due to the extra power consumption of completing the task. This implies that the power consumption can be derived by characterizing the difficulty index in the trajectory tracking. To proceed, we define the index of the moving difficulty. Let k denote the number of turning operations in a trajectory with the change of veering angle of the steering direction being $\pm 180^\circ$. Since the moving difficulty of the path is directly related to the path distance, we define the index as

$$\begin{aligned} difficulty \triangleq\ & (B_w D_w - 1)\hat{d} + \pi(D_w - 1)\hat{d}/2 \\ & + \left[(\pi/2 - 1)k + (\pi/4 - 1)\right. \\ & \left. \times (2D_w - 2k - 2)\right]\hat{d} \end{aligned} \tag{1}$$

where $k \in [1,\ D_w - 1]$, $\pi/2 - 1$ is a normalized distance difference between the turning navigation with the turning angle π and the straight navigation, $\pi/4 - 1$ is a normalized distance difference between the straight-line navigation and the turning navigation with the turning angle $\pi/2$, $(B_w D_w - 1)\hat{d}$ is a normalized distance of the whole straight navigation, $\pi(D_w - 1)\hat{d}/2$ is a normalized distance of the whole turning navigation, $[(\pi/2 - 1)k + (\pi/4 - 1)(2D_w - 2k - 2)]\hat{d}$ is a normalized distance difference between the whole turning and straight navigation, $B_w = L_l/\hat{d} - 1$ with L_l being an average length of the working area, $D_w = L_w/\hat{d} - 1$ with L_w being an average width of the working area, and $\hat{d} \in \mathbb{R}$ denotes a constant ratio between the unit m and 0.001 min. It can be concluded that the tracking the route with a larger k gives rise to higher moving difficulty from Eq. 1.

Since power consumption is roughly proportional to the moving difficulty (Eq. 1) under the same working efficiency, we define

$$p = p_0 \cdot difficulty \tag{2}$$

where $p_0 \in \mathbb{R}^+$. Equation 2 reveals that a larger k comes with more power consumption. In other words, tracking the trajectory with $k = 1$ reveals the minimal power consumption.

3.1 Preliminary Path Planning

Two terms—the time and energy consumption in the robot navigation—are defined here; "working

time" (denoted by T) represents the time consumed in the whole tracking task and "energy consumption" (stated as E) relates to the energy cost. The preliminary path planning sources with the objective of minimizing these two consumptions; it plans the optimal route in the off-line manner without obstacle avoidance. The word "preliminary" means that the obstacle avoidance is ignored in the current planning.

The preliminary strategy consists of the minimum time, minimum energy and mixed modes. First, given $T = E_0/p$ with Eq. 2 and E_0 denoting the constant energy consumption of tracking the route in the minimal time mode, the optimal path in current mode is specified as that with k being the solution of

$$\min_k T$$
$$\text{s.t.}$$
$$k \in [1, D_w - 1]$$

Note that T achieves its minimum when k is maximal.

Second, given $E = pT_0$ with the T_0 denoting the constant time consumption of tracking the route in the minimal energy mode, the optimal path in current mode is specified as that with k being the solution of

$$\min_k E$$
$$\text{s.t.}$$
$$k \in [1, D_w - 1]$$

Notice that E is minimal at $k = 1$.

Third, T and E must be redefined before we propose the mixed mode since T_0 and E_0 are inapplicable in the construction of the current mode; they are formulated by applying the following specifications: maximal traveling speed v, the maximal angular speed w_e, $t_c = V_d/m_1$ states the time cost of accelerating the motor to its maximal angular speed or decelerating the motor to zero, the slope of change for the motor's input voltage versus time t is m_1, and the maximal input voltage for the motor is V_d. Moreover, there are three variations: the variation of robot speed versus t from 0 to T_{sm} (i.e. the tracking time for the m–th straight-line navigation) in Fig. 1; the change of the angular speed versus t from 0 to T_{cm} (i.e. the time spent in the m–th turning navigation) in Fig. 2; and the variation of the input voltage versus t from 0 to T_v in Fig. 3. Given the variations in Figs. 1 and 2, we have $vt_c + v(T_{sm} - 2t_c) = l_m, w_e t_c + w_e(T_{cm} - 2t_c) = \theta_m$ where l_m and θ_m denote the distance and veering angle of the m–th straight-line and turning navigation, respectively. Then

$$T_{sm} = l_m/v + t_c,\ T_{cm} = \theta_m/w_e + t_c \tag{3}$$

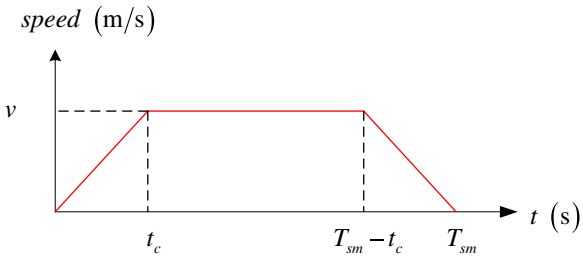

Fig. 1 Change of speed versus time during the straight navigation

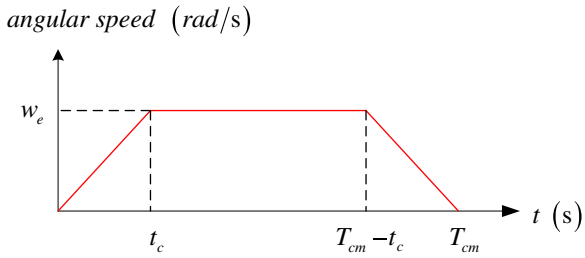

Fig. 2 Change of angular speed versus time during the turning navigation

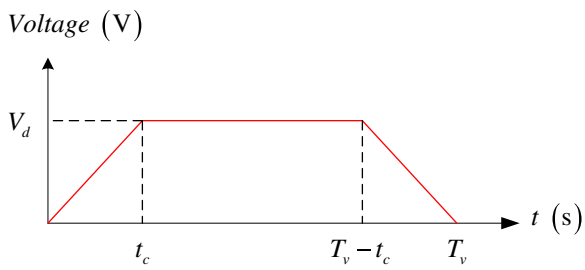

Fig. 3 Change of input voltage

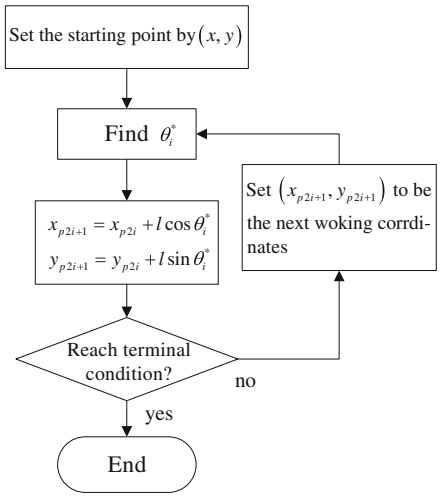

Fig. 4 Flowchart of refining the moving path

Setting $T_v = T_{sm}$ and $T_v = T_{cm}$ in Fig. 3 yields the energy consumption as

$$E_{sm} = \left[2\int_0^{t_c} m_1^2 t^2 dt + V_d^2\left(T_{sm} - 2t_c\right)\right]/R_i,$$

$$E_{cm} = \left[2\int_0^{t_c} m_1^2 t^2 dt + V_d^2\left(T_{cm} - 2t_c\right)\right]/R_i \qquad (4)$$

where E_{sm} and E_{cm} denote the energy consumed in the m–th straight and turning navigation, respectively, R_i is an equivalent inner resistance of the robot's motor, $2\int_0^{t_c} m_1^2 t^2 dt/R_i$ means the energy consumed in the motor acceleration and deceleration, $V_d^2(T_{sm} - 2t_c)/R_i$ is the energy consumption for the m–th straight-line navigation under constant speed v, and $V_d^2(T_{cm} - 2t_c)/R_i$ represents the energy consumed in the m–th turning navigation under constant angular speed w_e.

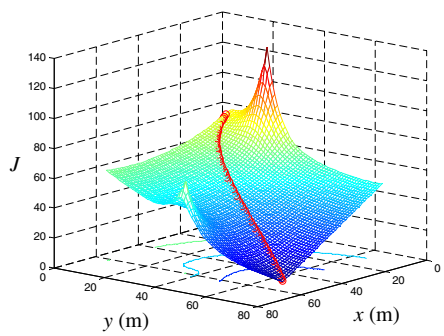

Fig. 5 Example of the cost field

Equations 3 and 4 are adopted to formulate the total time and energy consumption. While the number of the straight sections in the entire path is $N_s = 2D_w - k - 1$ and that of the veering sections is $N_c = 2D_w - k - 2$, combining (N_c, N_s) with Eq. 3 generates

$$T = l_T/v + \theta_T/w_e + \left(4D_w - 2k - 3\right)t_c \qquad (5)$$

where l_T/v is the total time for straight-line navigations, l_T is entire path length, θ_T/w_e represents the working time for all turning navigations, θ_T is sum of all turning angles, and $(4D_w - 2k - 3)t_c$ is extra working time induced by accelerating and decelerating the motors. Combining Eq. 4 with (N_c, N_s) yields

$$\begin{aligned} E = {} & 2\left(N_s + N_c\right)\int_0^{t_c} m_1^2 t^2 dt/R_i \\ & + V_d^2\left(T_{sm} - 2t_c\right)N_s/R_i \\ & + V_d^2\left(T_{cm} - 2t_c\right)N_c/R_i \end{aligned} \qquad (6)$$

where $V_d^2(T_{sm} - 2t_c)N_s/R_i$ is the energy consumed in the straight-line navigation under v, $V_d^2(T_{cm} - 2t_c)N_c/R_i$ is the energy spent in the turning navigation under w_e, and $(N_s + N_c)2\int_0^{t_c} m_1^2 t^2 dt/R_i$ relates to the energy consumption in the motor acceleration and deceleration. Substituting values of N_s and N_c into Eq. 6 generates

$$E = E_{c0} + 2km_1^2 t_c^3/3R_i \qquad (7)$$

where $E_{c0} = E\,|_{k=0}$. Equations 5 and 7 are further applied to derive the optimal path in the mixed mode.

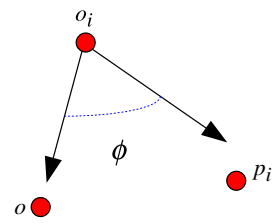

Fig. 6 Definition of the decreasing rate

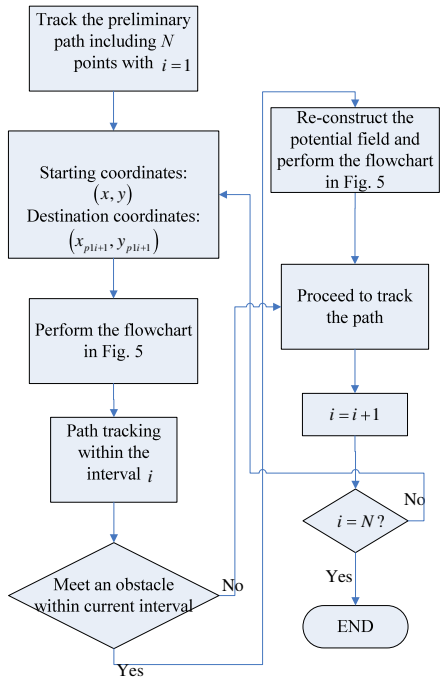

Fig. 7 Process of the path planning

To decide the optimal route in the mixed mode, we define an objective function $\widetilde{J}$ based on Eqs. 5 and 7.

$$\widetilde{J} = \left[\left(T_{c0}/A_w - 2kt_c\right)/T_{ma}\right]^2 + \left[\left(E_{c0} + 2km_1^2 t_c^3/3R_i\right)/E_{ma}\right]^2 \quad (8)$$

where A_w is a weighting factor, $T_{c0} = T|_{k=0}$, $E_{ma} = E|_{k=D_w-1}$, and $T_{ma} = T_{c0}/A_w - 2t_c$. The optimal route in the mixed mode is derived by solving the problem:

$$\min_k \widetilde{J}$$
s.t.
$$k \in [1,\, D_w - 1]$$

Performing $\partial\widetilde{J}/\partial k = 0$ gives the optimal k^* as

$$k^* = \text{ceil}\left(\frac{T_{c0}/A_w T_{ma}^2 + E_{c0}V_d^2/3R_i E_{ma}^2}{2t_c/T_{ma}^2 - 2V_d^4 t_c/9R_i^2 E_{ma}^2}\right) \quad (9)$$

where A_w is the solution of solving $\widetilde{J}(A_w, k)|_{k=1} = \widetilde{J}(A_w, k)|_{k=D_w-1}$, ceil$(x)$ is the ceiling function, which returns the smallest integer not less than x. The path revealing $k = k^*$ is treated as the optimal route in the mixed mode.

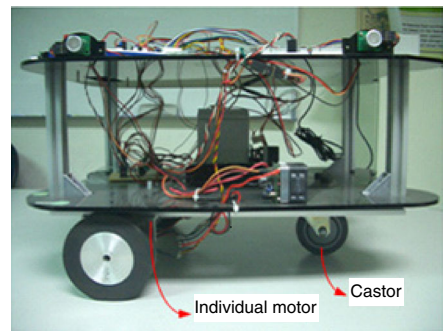

Fig. 8 Demonstration of the mobile robot

3.2 Obstacle and Robot Coordinates Computations

The optimal route has been proposed in a series of discrete points $(x_{p1i},\ y_{p1i})$ for $i = 1 \sim N$ after the preliminary trajectory planning. However, there are practical concerns—such as static or moving obstacles avoidance—that cannot be overlooked in the CCPP. The robot must take initiative to avoid these obstacles, located in advance or detected by the robot's sensors in the following way. Define the polar coordinates of the i-th sensor S_i with respect to the mass center of the whole platform are $(r_{si},\ \theta_{si})$. After S_i feedbacks the distance d_{si} between the detected obstacle and the robot, the obstacle coordinates are determined as $(x - (r_{si} + d_i)\sin(\theta + \theta_{si}),\ y - (r_{si} + d_i)\cos(\theta + \theta_{si}))$ where (x, y) are coordinates of the mass center of the platform, and θ is an angle between the moving direction and the longitudinal coordinate.

GPS has been used to locate the real-time position $(x,\ y)$ in this research. The two points p_a and p_b ($\overline{p_a p_b} < 1$ m) reveal the same GPS coordinates since the effective degree of GPS coordinates is 1 m. This gives rise to the requirement of establishing a precisely positioning strategy for $(x,\ y)$. Given $t_b > t_a > 0$, the robot position at time t_b is determined as $(x, y) = (x_{gps} + \int_{t_a}^{t_b}\Delta L(t)\cos\theta(t)dt,\ y_{gps} + \int_{t_a}^{t_b}\Delta L(t)\sin\theta(t)dt)$ where $(x_{gps},\ y_{gps})$ are the GPS coordinates at time t_a and $\Delta L(t)$ denotes the accumulated mileage from t–Δt to t. This reduces the positioning error of GPS.

Given the precise position $(x,\ y)$ and moving object location, its moving speed is approximated

Table 1 Specification of the autonomous robot

Part	Specification
DC motor	IG-42GM 12V
Encoder	HB-25 with maximum input current 25A
Battery	12 V, 5 Ah
Rear wheel	Diameter:10 cm
Caster	Diameter:7 cm
Vehicle weight and height	9.7 kg and 25 cm

Table 2 Sensors' specifications

Sensor	Output	Type
Gyrometer	Yaw angle	IDG-300
GPS receiver	GPS coordinates	GPS 35
Ultrasonic sensors	Distance between the vehicle and an obstacle within [15, 600] (cm)	Srf02
Encoder	Angular velocity	HB-25

as $\sqrt{(x_{omt2}-x_{omt1})^2+(y_{omt2}-y_{omt1})^2}/(t_2-t_1)$, $t_2>t_1$ where the coordinates of the i-th obstacle at time t_1 and t_2 are detected as (x_{omt1}, y_{mit1}) and (x_{omt2}, y_{omt2}), respectively, and the moving direction is from (x_{omt1}, y_{omt1}) to (x_{omt2}, y_{omt2}).

3.3 On-Line Path Planning with Fixed Obstacle Avoidance

While Sisbot et al. [27] have proposed a potential field method to design the robot path featuring the obstacle avoidance, it is inapplicable in our CCPP considering the moving objects avoidance since the method of [27] is only suitable for the static obstacles. Therefore, we improve the strategy for the obstacle avoidance design of the moving and fixed objects. Let us consider the case of the fixed objects first.

Modifying the preliminary path by the improved potential field processes the function of the obstacle avoidance. For convenience, we only demonstrate the modification at the $(j-1)$-th interval of the preliminary path, in which the starting point and the destination are (x, y) and (x_{p1j}, y_{p1j}), respectively. The modification is performed by applying working dangerousness and difficulty indices. First of all, we propose the working dangerousness index by the concern—the closer the robot is to the obstacle, the more dangerousness it will be. This can be represented as

$$danger_i \triangleq \sum_{j=1}^{n} \hat{h}_j r^{\|\bar{z}\|},\ \bar{z} = \left[\, x_{p2i} - x_{oj}\ y_{p2i} - y_{oj} \,\right]^T \tag{10}$$

where (x_{p2i}, y_{p2i}) is the presently selected route coordinates, $\hat{h}_j$ represents the degree of dangerousness at the mass center (x_{0i}, y_{0i}) of the static obstacle, $r^{\|\bar{z}\|}$ with $0 < r < 1$ represents a decreasing rate of the danger strength, and n represents number of obstacles. The strength of $danger_i$ states the repelling force of the obstacle. Secondly, the working difficulty index is constructed to smooth the avoiding trajectory; it is described as

$$difficulty_i \triangleq \|\bar{z}\|,\ \bar{z} = \left[\, x_{p2i} - x_{p1j}\ y_{p2i} - y_{p1j} \,\right]^T \tag{11}$$

since the working difficulty is essentially proportional to the trajectory distance. Equation 11 implies that the closer the robot to the destination is, the easier the navigation work will be. Inverse of $difficulty_i$ means the attractive force produced by the destination.

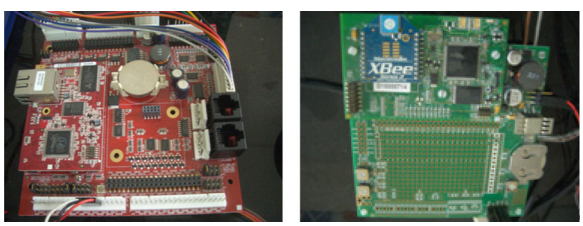

(a) (b)

Fig. 9 Embedded system boards, **a** BL2600, **b** RCM4510

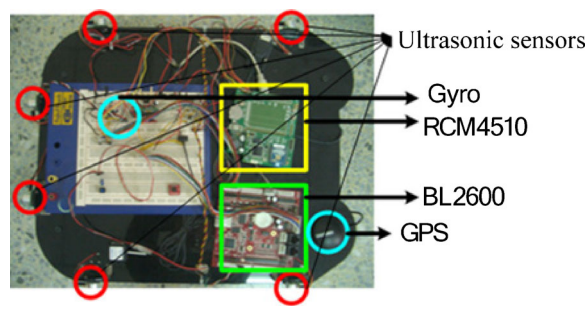

Fig. 10 Arrangement of sensors

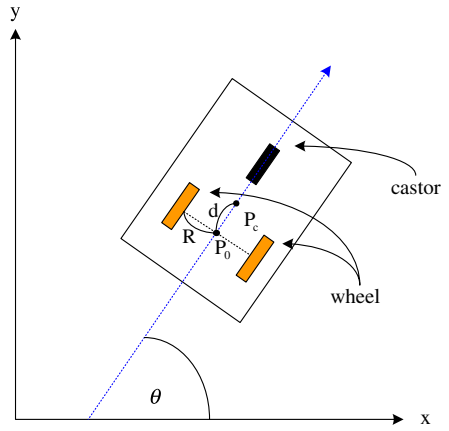

Fig. 11 Autonomous robot

The potential field of refining the preliminary trajectory is constructed with the working dangerousness and difficulty indices. Combining Eqs.10 and 11 forms

$$J_i = \rho\, difficulty_i + (1-\rho)\, danger_i,\ \ \rho \in [0,1] \quad (12)$$

where J_i reflects the strength of the potential field at $(x_{p2i},\ y_{p2i})$, and ρ denotes a weighting factor. Searching for the minimum cost path with the given starting position by the flowchart in Fig. 4 generates the modified route within the current interval. In this flowchart, the next path point is determined as $P_{pi} = \left(x + l\cos\theta_i^*,\ y + l\sin\theta_i^*\right)$ where the robot's position is $P_c(x,\ y)$, l specifies the unit incremental path length, and θ_i^* is the solution of

$$\min_{\theta_i \in [0,2\pi]} J_i\left(x + l\cos\theta_i,\ y + l\sin\theta_i\right)$$

with θ_i being an angle between the vector and the wheel's axis of the robot. The progress in Fig. 4 terminates when the length of $\langle x_{p2i+1} - x_{p1j},\ y_{p2i+1} - y_{p1j}\rangle$ is less than l. Figure 5 demonstrates an example of the potential field with $\rho = 0.5$ in which the line denotes the modified route computed by the flowchart in Fig. 4.

Table 3 System parameters' definitions

Parameter	Definition
m, m_w	Mass of the whole platform and wheel
I_w, I_p	Moment of inertia of each wheel and whole platform
p_c, p_0	Mass center of the whole platform and the center between two wheels' axis
d	Distance between p_c and p_0
R	Distance between the wheel's axis and p_0

Table 4 System parameters' settings

Parameter	Setting
m, m_w	9.7 kg, 0.3 kg
I_w, I_p	0.00075 kg-m^2, 0.2354 kg-m^2
h_1, d, R	0.05 m, 0.09 m, 0.176 m
$\tau_{\max}$	0.18 kg-m
$\hat{d}$	1 (m/mmin)
l, r	0.1, 0.9
(r_{01}, r_{02})	(0.5, 0.1)

3.4 On-Line Path Planning with Moving Obstacle Avoidance

Humans, stayed in the working field, might be threatened by the working robot. Therefore, how to simultaneously ensure high human safety in the robot navigation must be considered in CCPP due to the safety concern. This is fulfilled by designing the robot motions based on an index of the human safety. Since the longer distance from the robot to human is, the higher safety will be, this leads to an index of the human safety at the waypoint $(x_{p2i},\ y_{p2i})$ as $1/danger_i$. To establish the robot route revealing high human safety, let us treat humans as moving objects in the environment and avoid them.

The optimal path design of avoiding moving object and simultaneously guaranteeing the human safety is presented. Since the smaller $1/danger_i$ indicates that the object is threatened by the robot, r in Eq. 10 must be large enough to make the robot far away from the object when it is in the invisible zone behind the object. It is redefined as

$$r = r_{01}\,|\cos(\phi/2)| + r_{02} \quad (13)$$

where $r_{01},\ r_{02} \in (0,1)$, ϕ is a angle between $\overrightarrow{o_i o}$ and $\overrightarrow{o_i p_i}$ (see Fig. 6), $o(x_o,\ y_o)$ represents previous coordinates of the moving object, $o_i(x_{oi},\ y_{oi})$ is current position of the moving object, and p_i states present robot position. The term $r_{01}\,|\cos(\phi/2)|$ in Eq. 13 increases r such that its maximum appears at $\phi = 0$ (that is, the invisible zone behind the

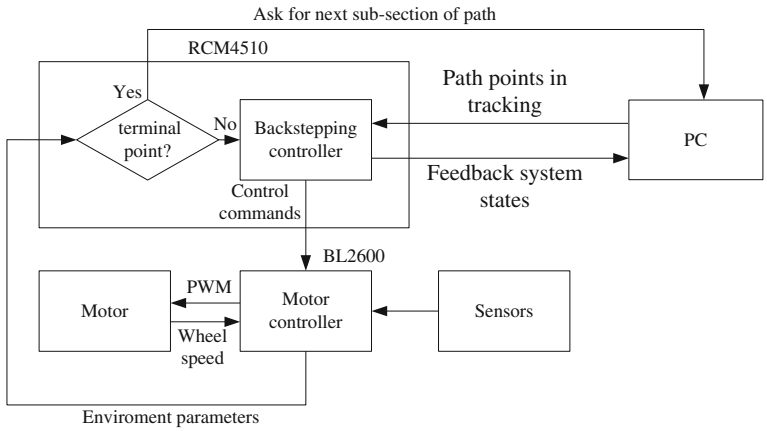

Fig. 12 Flowchart of the path tracking

object). That is, the robot becomes the farthest away from the object when it is in the invisible zone behind the object. This increases the human safety.

Figure 7 displays the flowchart of the on-line path planner which has involved the process of Fig. 4. If the robot encounters an obstacle at the i-th interval, it will avoid the obstacle via the flowchart in Fig. 4 with the starting position and destination being the robot position (x, y) in the navigation and the $(i+1)$-th waypoint (x_{p1i+1}, y_{p1i+1}) of the preliminary path. The effect of the tracking errors on the human safety in the robot navigation are considered in the on-line manner by treating the starting point in the potential field as (x, y) instead of (x_{p1i}, y_{p1i}). The process in Fig. 7 is continued until all of the preliminary path waypoints are passed.

Despite the obstacle avoidance strategy of our previous work [26] was referred in the current approach, the latter is slightly different in that the objective field of designing the trajectory of the obstacle avoidance is constructed at the real robot position instead of (x_{p1i}, y_{p1i}) in [26]. This makes the robot to be aware of the humans around in its navigation and thus guarantees human safety.

4 Tracking Control Design

The objective of this section is to propose a tracking controller for the robot equipped with two individual motors, a differential drive and a castor; see Fig. 8 for illustration.

4.1 System Modeling

Consider the kinetic model of [28] for the wheeled robot as

$$M(q)\ddot{q} + C(q, \dot{q}) = E_c\tau - A^T(q)\lambda \tag{14}$$

where $q = \left[\, x\ y\ \theta\ \theta_r\ \theta_l \,\right]^T$ is a system state, θ_r and θ_l are turning angles of the right and left wheels, $M \in \mathbb{R}^{5\times5}$, $C \in \mathbb{R}^{5\times1}$, $\lambda \in \mathbb{R}$ is a Lagrange multiplier, $A \in \mathbb{R}^{n_c\times5}$ with n_c being a number of the nonholonomic constraints described by $A(q)\dot{q} = 0$, $\tau = \left[\, \tau_r\ \tau_l \,\right]^T$ with τ_r and τ_l being torques added to the right and left motors, and

$$E_c = \begin{bmatrix} 0\ 0\ 0\ 1\ 0 \\ 0\ 0\ 0\ 0\ 1 \end{bmatrix}^T$$

Table 5 Results for the minimal time mode

Scenario	Consumed power (W)
No obstacles	0.0498
Three fixed, one moving	0.0703

Table 6 Results for the minimal energy mode

Scenario	Consumed power (W)
No obstacles	0.0338
Three fixed, one moving	0.0629

Table 7 Results for the mixed mode

Scenario	Consumed power (W)
No obstacles	0.0433
Three fixed, one moving	0.0649

Yamamoto et al. [28] supposed that there exists a matrix $S \in \mathbb{R}^{5\times 2}$ such that $A(q)\,S = 0$. That is,

$$\dot{q} = Sz \tag{15}$$

where $z = [z_1\ z_2]^T$ denotes angular velocities of the right and left wheels. To linearize the kinetic model (Eq. 14), we propose a nonlinear control law

$$\tau(u) = \left(S^T E_c\right)^{-1} S^T M S \times \left[u + \left(S^T M S\right)^{-1}\left(S^T M \dot{S} z + S^T C\right)\right] \tag{16}$$

where the input $u = \left[u_1\ u_2\right]^T$ reflects the angular accelerations of the wheels. After one substitutes Eq. 16 into Eq. 14, combining the linearized system of Eq. 14 with Eq. 15 yields

$$\begin{bmatrix} \dot{q} \\ \dot{z} \end{bmatrix} = \begin{bmatrix} 0 & S \\ 0 & 0 \end{bmatrix} \begin{bmatrix} q \\ z \end{bmatrix} + \begin{bmatrix} 0 \\ I_2 \end{bmatrix} u \tag{17}$$

which is considered in the control design.

4.2 Control Design

The control strategy is presented with objective of enabling the robot (Eq. 17) to track the optimal route. Since q in Eq. 17 is directly affected by z which is determined by u, backstepping strategy appears to be an available idea to simplify the design of u with the nonlinear control law (Eq. 16).

Performing point stabilizations for the path points of the robot route sequentially completes the whole tracking task. For convenience, we only demonstrate the point stabilization at a given interval between the starting point $(x_s,\ y_s)$ and destination (x_d, y_d) (these two points belong to the path points). A reference trajectory, described by an ideal kinetic model, of the point stabilization is proposed to prevent the robot from working outside the workspace in advance. Consider $\left(\dot{x}, \dot{y}, \dot{\theta}\right)$ of Eq. 15 as

$$\dot{x} = f_1(q, z_d),\ \dot{y} = f_2(q, z_d),\ \dot{\theta} = f_3(q, z_d) \tag{18}$$

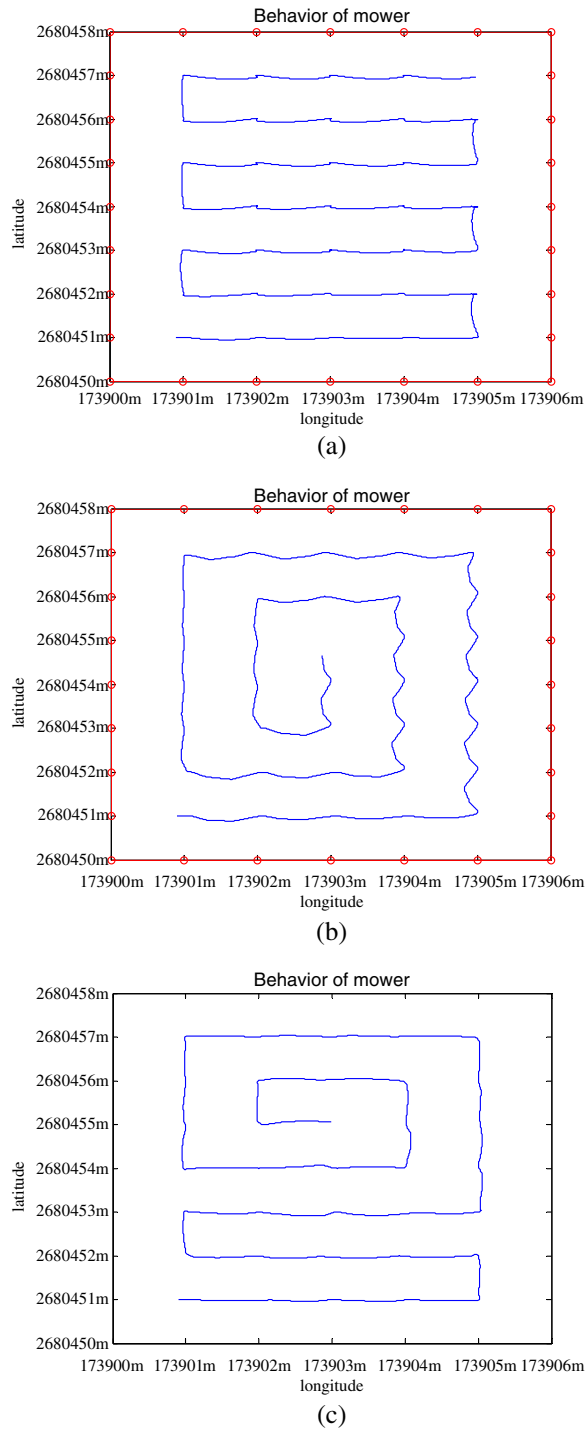

Fig. 13 Verification results without obstacles existing in the field, **a** minimal time mode, **b** minimal energy mode, **c** mixed mode

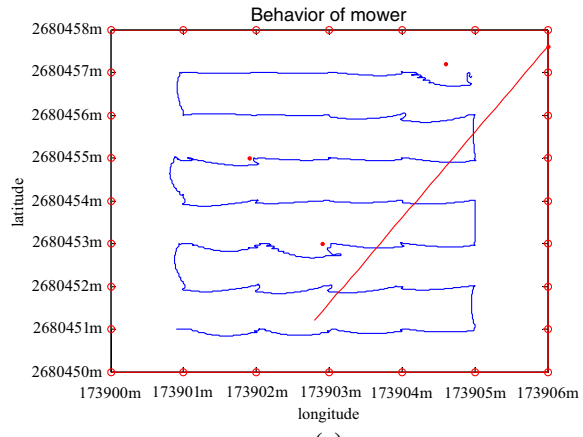

(a)

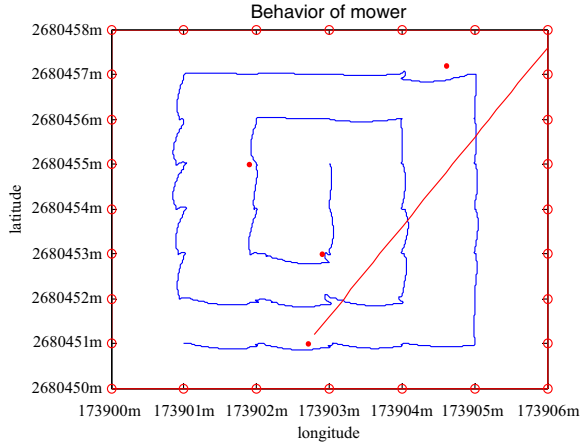

(b)

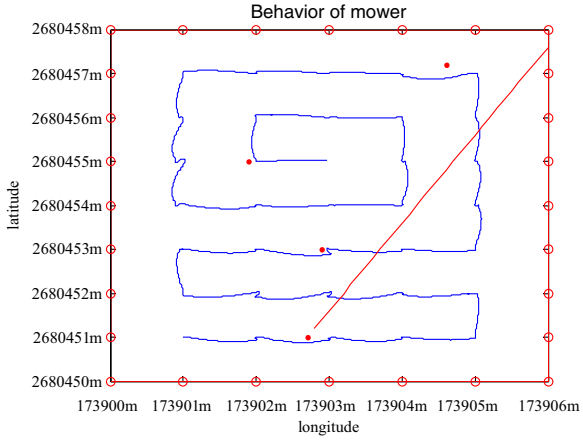

(c)

Fig. 14 Results with fixed and moving objects existing in the working field, **a** minimal time mode, **b** minimal energy mode, **c** mixed mode

where $f_i : \mathbb{R}^{5\times 2} \to \mathbb{R}$ for $i = 1 \sim 3$ are smooth functions with respect to their arguments, $z = z_d = \left[\, z_{1d}\ z_{2d} \,\right]^T$ represents the pseudo-input command. Referring to the kinetic model in [29], we propose the ideal model of Eq. 18:

$$\dot{x}_R = f_1\left(q_R, z_R\right), \dot{y}_R = f_2\left(q_R, z_R\right), \\ \dot{\theta}_R = f_3\left(q_R, z_R\right) \tag{19}$$

where $z_R = [z_{1R} z_{2R}]$ with $z_{1,2R} = v_0\sqrt{(x_R - s_d)^2 + (y_R - y_d)^2}$, $v_0 \in \mathbb{R}^+$ and $q_R = [\, x_R\ y_R\ \theta_R\ \theta_{rR}\ \theta_{lR}\,]^T$ are ideal values corresponding to z_d and q, respectively, and the initial θ_R satisfies $\tan\theta_R = (y_d - y_s)/(x_d - x_s)$. Evaluating $z_{1,2R}$ in Eq. 19 with the same value lets the reference robot move toward the destination. This implies that tracking the reference route (Eq. 19) accomplishes the point stabilization.

Tracking errors are denoted by $e_x = x - x_R$, $e_y = y - y_R$, $e_\theta = \theta - \theta_R$ with

$$\dot{e}_x = f_1\left(q, z_d\right) - f_1\left(q_R, z_R\right) \triangleq \alpha_1\left(z_d\right), \\ \dot{e}_y = f_2\left(q, z_d\right) - f_2\left(q_R, z_R\right) \triangleq \alpha_2\left(z_d\right) \tag{20}$$

If the robot approaches $(x_R,\ y_R)$, θ may converge to θ_R. This inspires a Lyapunov function candidate $V_1 = 0.5(e_x^2 + e_y^2)$ with $V_1 \to \infty$ as $\|[\, e_x\ e_y\,]\| \to \infty$ and $\dot{V}_1 = e_x\alpha_1(z_d) + e_y\alpha_2(z_d)$ where

$$\alpha_1\left(z_d\right) = \alpha_{1x}\left(q, q_R\right) z_{1d} + \alpha_{2x}\left(q, q_R\right) z_{2d} \\ + \alpha_{3x}\left(q, q_R, z_R\right), \\ \alpha_2\left(z_d\right) = \alpha_{1y}\left(q, q_R\right) z_{1d} + \alpha_{2y}\left(q, q_R\right) z_{2d} \\ + \alpha_{3y}\left(q, q_R, z_R\right) \tag{21}$$

The system (Eq. 20) would be globally asymptotically stable since $\dot{V}_1 = -ck_1e_x^2 - ck_2e_y^2 < 0$ is ensured by determining $\alpha_1\left(z_d\right) = -k_1e_x$ and $\alpha_2\left(z_d\right) = -k_2e_y$. Substituting $\alpha_1\left(z_d\right) = -k_1e_x$ and $\alpha_2\left(z_d\right) = -k_2e_y$ into Eq. 21 yields

$$z_{1d} = \left(-\alpha_{2y}k_1e_x - \alpha_{2y}\alpha_{3x} + \alpha_{2x}k_2e_y + \alpha_{2x}\alpha_{3y}\right) \\ / \left(\alpha_{1x}\alpha_{2y} - \alpha_{1y}\alpha_{2x}\right), \\ z_{2d} = \left(-\alpha_{1x}k_2e_y - \alpha_{1x}\alpha_{3y} + \alpha_{1y}k_1e_x + \alpha_{1y}\alpha_{3x}\right) \\ / \left(\alpha_{1x}\alpha_{2y} - \alpha_{1y}\alpha_{2x}\right) \tag{22}$$

This states the desired angular velocities z_d of Eq. 18.

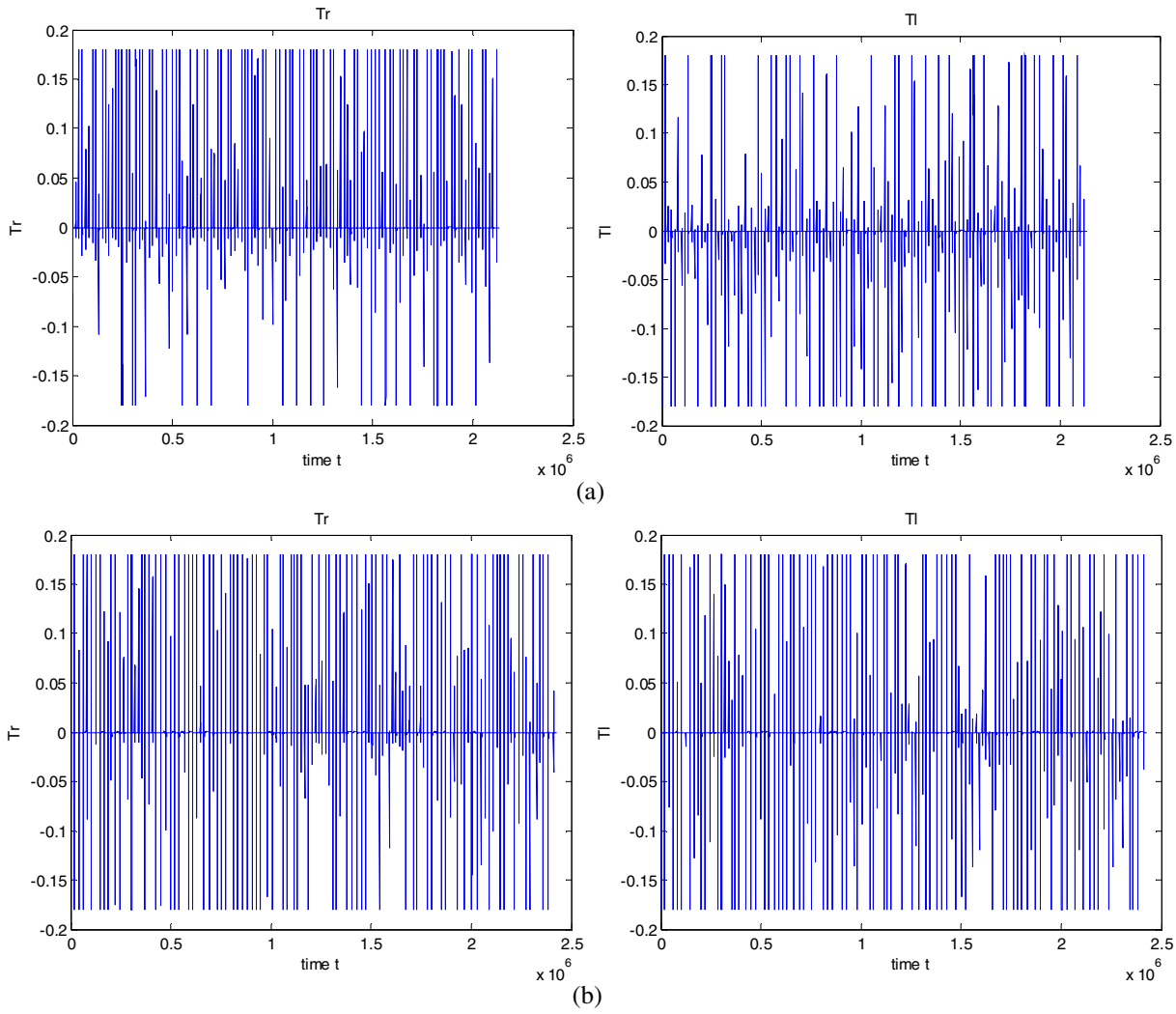

Fig. 15 Control input in minimum time mode, **a** torques added to the motors without obstacles, **b** torques added to the motors considering fixed and moving obstacles

u is designed next to make z track $z_d = \left[z_{1d}\ z_{2d} \right]^T$ upon $\dot{z} = u$ in Eq. 17 under a constraint $\|\tau\| \leq \tau_{\max}$. First, we propose u while releasing the constraint. Define the tracking error $e_z = z - z_d = [\, e_{z_1}\ e_{z_2}\,]^T$ with

$$\dot{e}_z = u - \dot{z}_d \tag{23}$$

A Lyapunov function candidate is further determined by $V_2 = (e_{z1}^2 + e_{z2}^2 + e_x^2 + e_y^2)/2$ with

$$\dot{V}_2 = -k_1 e_x^2 - k_2 e_y^2 + e_{z1}\left(u_1 - \dot{z}_{1d} + \alpha_{1x} e_x + \alpha_{1y} e_y\right) + e_{z2}\left(u_2 - \dot{z}_{2d} + \alpha_{2x} e_x + \alpha_{2y} e_y\right) \tag{24}$$

where $\dot{V}_2 < 0$ if

$$u_1 = \dot{z}_{1d} - \alpha_{1x} e_x - \alpha_{1y} e_y - \overline{k}_1 (z_1 - z_{1d}),$$
$$u_2 = \dot{z}_{2d} - \alpha_{2x} e_x - \alpha_{2y} e_y - \overline{k}_2 (z_2 - z_{2d}) \tag{25}$$

with $\overline{k}_{1,2} \in \mathbb{R}^+$. The system (Eq. 23) will be globally asymptotically stable since $V_2 \to \infty$ as $\|[\, e_{z1}\ e_{z2}\ e_x\ e_y\,]\| \to \infty$.

Second, τ of Eq. 16 is reconstructed such that $\|\tau\| \leq \tau_{\max}$ while the system (Eq. 23) remains its stability. Given $\hat{\tau} = [\, \hat{\tau}_r\ \hat{\tau}_l\,]^T = \tau(u_1, u_2)$ in Eq. 16 with (u_1, u_2) of Eq. 25, the reconstruction of τ is divided into those with $\|\hat{\tau}\| \leq \tau_{\max}$ and $\|\hat{\tau}\| > \tau_{\max}$. Consider $\|\hat{\tau}\| \leq \tau_{\max}$. It was

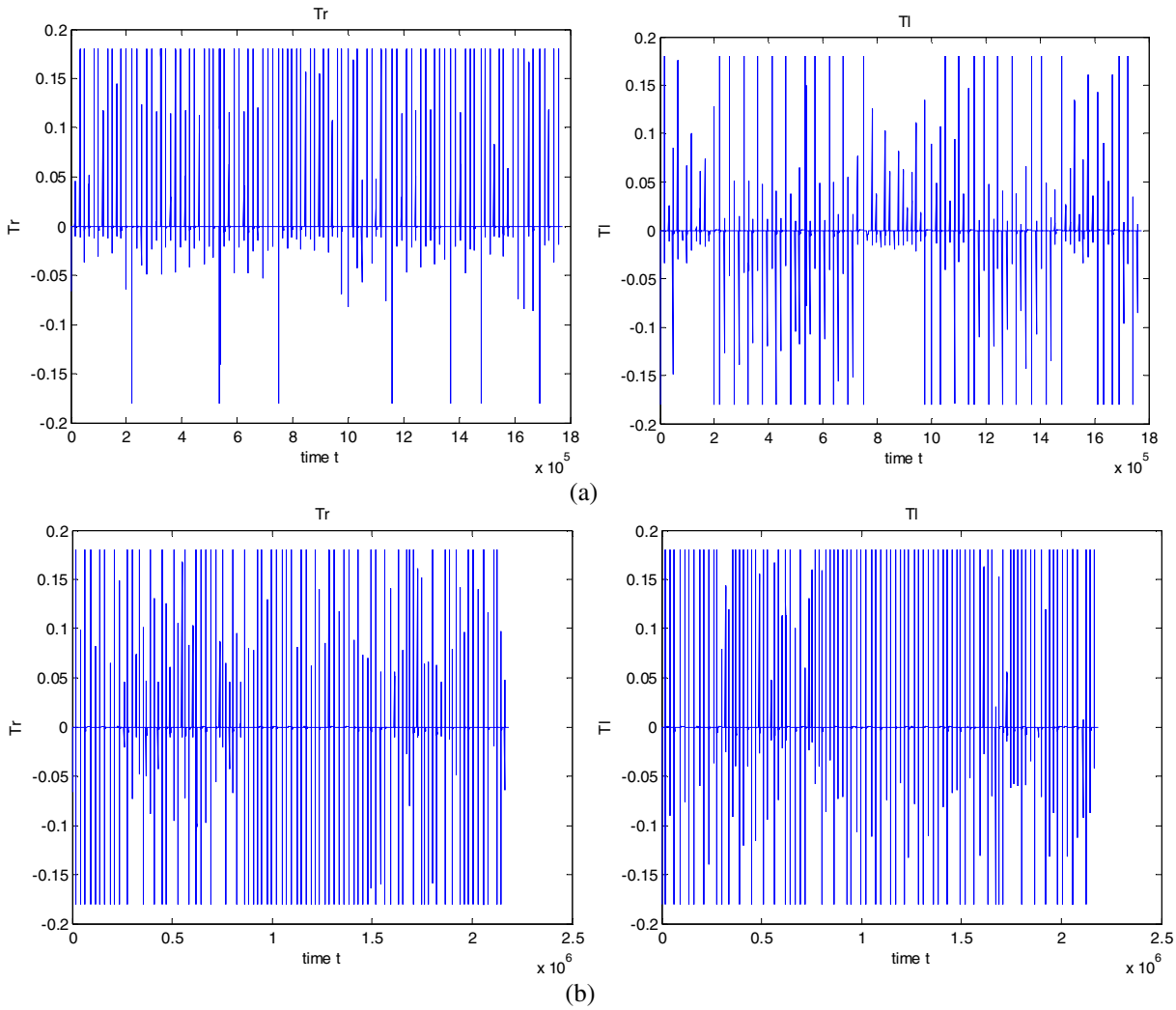

Fig. 16 Control input in minimum energy mode, **a** torques added to the motors without obstacles, **b** torques added to the motors considering fixed and moving obstacles

proved that the system (Eq. 23) is globally asymptotically stable if $\tau = \hat{\tau}$. On the contrary, if $\|\hat{\tau}\| > \tau_{\max}$, minimizing the second and third terms in Eq. 24 subject to the constraint $\|\tau(u)\| \leq \tau_{\max}$ leads to $\dot{V}_2 < 0$. This is performed by an objective function $\hat{J}(u_1, u_2) = \hat{J}_1(u_1) + \hat{J}_2(u_2)$ based on Eq. 24 where $\hat{J}_1 = e_{z1}^2(u_1 - \dot{z}_{1d} + \alpha_{1x}e_x + \alpha_{1y}e_y)^2$, $\hat{J}_2 = e_{z2}^2(u_2 - \dot{z}_{2d} + \alpha_{2x}e_x + \alpha_{2y}e_y)^2$, and $(u_1,\ u_2)$ satisfies

$$\hat{J}_1(u_1) \geq \hat{J}_1\left(\dot{z}_{1d} - \alpha_{1x}e_x - \alpha_{1y}e_y - \overline{k}_1 e_{z1}\right),$$
$$\hat{J}_2(u_2) \geq \hat{J}_2\left(\dot{z}_{2d} - \alpha_{2x}e_x - \alpha_{2y}e_y - \overline{k}_2 e_{z2}\right)$$

Solving the constrained optimization problem

$$\min_{\tau} \hat{J}$$
$$\text{s.t.}$$
$$\|\tau\| \leq \tau_{\max},$$
$$\hat{J}_1(u_1) \geq \hat{J}_1\left(\dot{z}_{1d} - \alpha_{1x}e_x - \alpha_{1y}e_y - \overline{k}_1 e_{z1}\right),$$
$$\hat{J}_2(u_2) \geq \hat{J}_2\left(\dot{z}_{2d} - \alpha_{2x}e_x - \alpha_{2y}e_y - \overline{k}_2 e_{z2}\right)$$

generates $\tau = \left[\tau_{\max} sgn\left(\tau_r^*\right)\ \tau_{\max} sgn\left(\tau_l^*\right)\right]$ where $\tau^* = \tau\left(u_1^*, u_2^*\right)$ with $\left(u_1^*, u_2^*\right)$ being of the form (Eq. 25) and the minimal solution of $\hat{J}$. $\dot{V}_2 < 0$

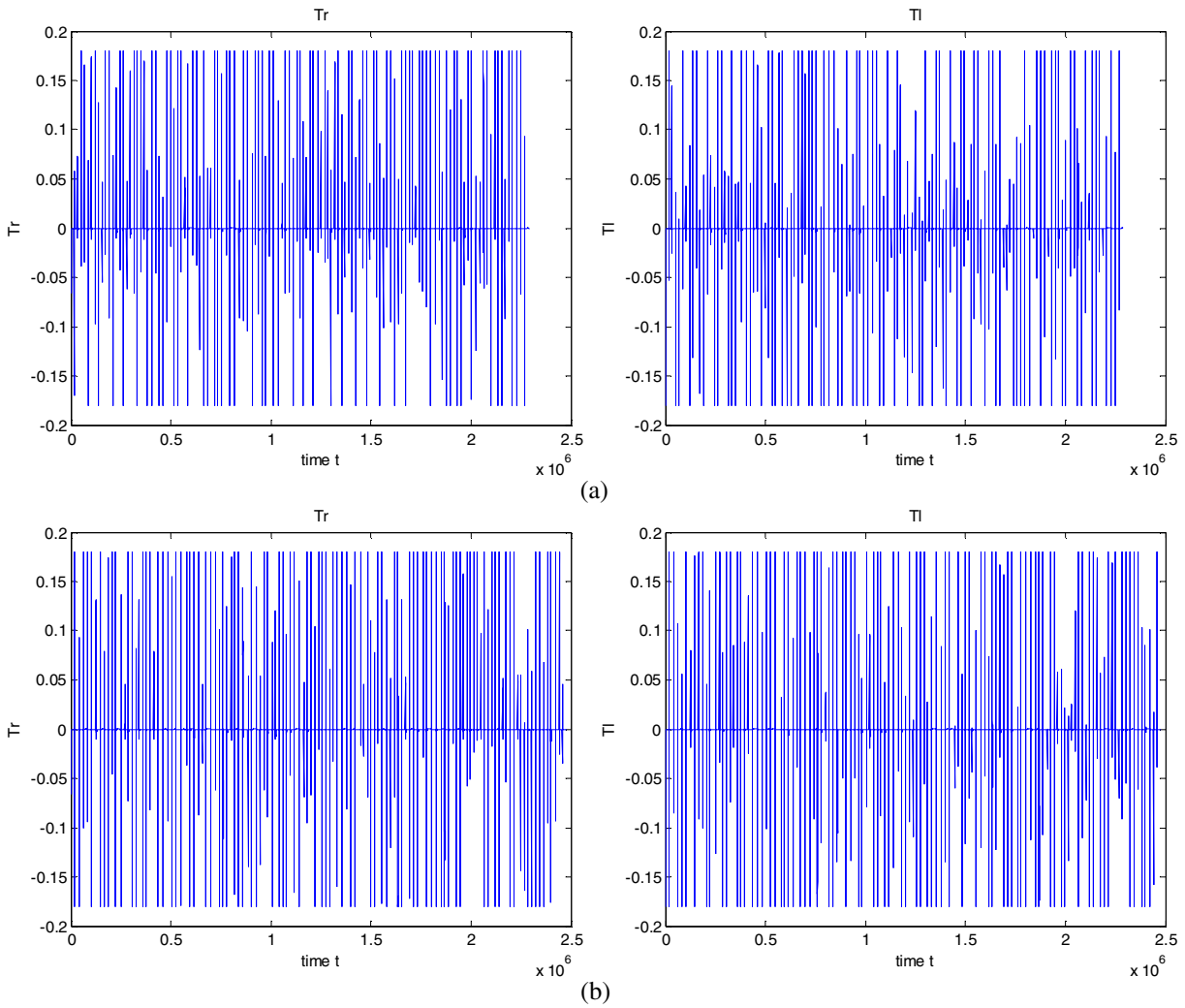

Fig. 17 Control input in mixed mode, **a** torques added to the motors without obstacles, **b** torques added to the motors considering fixed and moving obstacles

is thus achieved. The system (Eq. 23) is globally asymptotically stable under $\|\hat{\tau}\| > \tau_{\max}$ since $V_2 \to \infty$ as $\left\| \left[e_{z1}\ e_{z2}\ e_x\ e_y \right]^T \right\| \to \infty$.

Table 8 Parameter settings

Parameter	Value
T_{c0}	50.6711 s
E_{ma}, E_{c0}	752.1062 J, 688.1062 J
T_{ma}, t_c	2.533 s, 0.5 s
A_w	14.34
V_d	12 V
R_i	6 Ω

According to the above discussion, the backstepping controller is finally proposed as

$$\tau_{r,l} = \begin{cases} \tau_{\max}, & \text{if } \hat{\tau}_{r,l} > \tau_{\max}, \\ \hat{\tau}_{r,l}, & \text{if } \left|\hat{\tau}_{r,l}\right| \le \tau_{\max}, \\ -\tau_{\max}, & \text{if } \hat{\tau}_{r,l} < -\tau_{\max} \end{cases} \tag{26}$$

which initially works like a bang-bang controller while $\|\hat{\tau}\| > \tau_{\max}$. After the tracking error reaches within a tolerable range, Eq. 26 becomes the backstepping type ensuring satisfactorily tracking performance.

5 Demonstration and Results

5.1 Introduction of the Vehicle

The mobile robot, considered in the verification, consists of the hardware including an acrylic-based framework with two individually motorized wheels with encoders; a caster in its rear; an embedded system on the platform; and six ultrasonic sensors around the platform. Please see Fig. 8 and Table 1 for this robot and its specifications. The functions of the robot's devices are explained below.

1) *Two Embedded Boards:* The tracking controller was realized in RCM4510 (see Fig. 9b), which sent the control commends to BL2600 (Fig. 9a) adopted to generate the PWM signals according to the control commands. All sensory data were sent to BL2600 and further transmitted to RCM4510 for further processing.
2) *GPS Receiver:* The GPS receiver (see Table 2 for its specifications) supporting the data protocol NEMA 0183 was implemented to locate the robot. The value corresponding to the unit 10^{-4} min in GPS information was omitted for convenience of presentation since the effective degree of the GPS coordinates is 10^{-3} min.
3) *Ultrasonic Sensors:* Six ultrasonic sensors, which are specified in Table 2, were set up around the robot's edge (see Fig. 10) to detect the distance between the vehicle and the obstacle.
4) *Gyro and Encoders:* The yaw angle of the robot was computed by the gyro as listed in Table 2. Moreover, the encoder (see Table 2 for its specifications) was applied to calculate the accumulated mileage $2\pi h_1 N_T$ for the robot, where h_1 and N_T are radius and accumulated rotation times of the wheel.

5.2 Kinetic Model

The kinetic robot model (Fig. 11), considered in the experiment, in terms of the physical parameters listed in Table 3 is established in this section with three constraints [28]: 1) the vehicle moves forward at any instance; 2) no sliding on the right wheel; and 3) no sliding on the left wheel. These constraints can be augmented in the matrix representation as

$$A(\theta)\,\dot{q} = 0 \tag{27}$$

where

$$A(\theta) = \begin{bmatrix} \sin\theta & -\cos\theta & d & 0 & 0 \\ \cos\theta & \sin\theta & R & -h_1 & 0 \\ \cos\theta & \sin\theta & -R & 0 & -h_1 \end{bmatrix}$$

and the solution of Eq. 27 is determined as Eq. 15 with

$$S = \begin{bmatrix} c(R\cos\theta - d\sin\theta) & c(R\cos\theta + d\sin\theta) \\ c(R\sin\theta + d\cos\theta) & c(R\sin\theta - d\cos\theta) \\ c & -c \\ 1 & 0 \\ 0 & 1 \end{bmatrix},$$

$$c = h_1/2R \tag{28}$$

The kinetic model of the form (Eq. 14) and subject to Eq. 27 is derived by using Lagrange equation. Given $E_w = [I_w^2\dot{\theta}_r^2 + I_w\dot{\theta}_l^2 + m_w(h_1\dot{\theta}_r)^2 + m_w(h_1\dot{\theta}_l)^2]/2$ denotes the kinetic energy function of the wheels with respect to their mass centers and $E_p = \{m[\dot{x} + h_1(\dot{\theta}_r + \dot{\theta}_l)\cos\theta]^2 + m[\dot{y} + h_1(\dot{\theta}_r + \dot{\theta}_l)\sin\theta]^2 + I_p\dot{\theta}^2\}/2$ states the energy function of the platform with respect to p_c, the corresponding Lagrange equation is proposed as $L = E_p + E_w$. Combining

$$\frac{d}{dt}\left(\frac{\partial L}{\partial \dot{x}}\right) - \frac{\partial L}{\partial x} = 0,\ \frac{d}{dt}\left(\frac{\partial L}{\partial \dot{y}}\right) - \frac{\partial L}{\partial y} = 0,\ \frac{d}{dt}\left(\frac{\partial L}{\partial \dot{\theta}}\right) - \frac{\partial L}{\partial \theta} = 0,$$

$$\frac{d}{dt}\left(\frac{\partial L}{\partial \dot{\theta}_r}\right) - \frac{\partial L}{\partial \theta_r} = \tau_r,\ \frac{d}{dt}\left(\frac{\partial L}{\partial \dot{\theta}_l}\right) - \frac{\partial L}{\partial \theta_l} = \tau_l \tag{29}$$

with Eq. 27 generates Eq. 14 where

$$M = \begin{bmatrix} m & 0 & 0 & -mh_1\cos\theta & -mh_1\cos\theta \\ 0 & m & 0 & -mh_1\sin\theta & -mh_1\sin\theta \\ 0 & 0 & I_p & 0 & 0 \\ -mh_1\cos\theta & -mh_1\sin\theta & 0 & mh_1^2 + I_w + m_w h_1^2 & mh_1^2 \\ -mh_1\cos\theta & -mh_1\sin\theta & 0 & mh_1^2 & mh_1^2 + I_w + m_w h_1^2 \end{bmatrix},$$

$$C = \begin{bmatrix} mh_1\left(\dot{\theta}_r + \dot{\theta}_l\right)\dot{\theta}\sin\theta \\ -mh_1\left(\dot{theta}_r + \dot{\theta}_l\right)\dot{\theta}\cos\theta \\ -m\dot{x}h_1\left(\dot{\theta}_r + \dot{\theta}_l\right)\sin\theta + mh_1\dot{y}\left(\dot{\theta}_r + \dot{\theta}_l\right)\cos\theta \\ m\dot{x}h_1\dot{\theta}\sin\theta - m\dot{y}h_1\dot{theta}\cos\theta \\ m\dot{x}h_1\dot{\theta}\sin\theta - m\dot{y}h_1\dot{\theta}\cos\theta \end{bmatrix}$$

For this system, substituting S of Eq. 28 into its linearized version (Eq. 17) finally yields the constrained kinetic model in the verification.

5.3 Experiments

Verification of the proposed CCPP was conducted with the experimental robot (see Fig. 8) equipped with the controller (Eq. 26) in which the parameters were evaluated by expanding Eq. 15 with S in Eq. 28:

$$\begin{aligned}
\alpha_{1x} &= c\cos(\theta_R + \theta_0)\cos e_\theta - c\sin(\theta_R + \theta_0)\sin e_\theta, \\
\alpha_{2x} &= c\cos(\theta_R - \theta_0)\cos e_\theta - c\sin(\theta_R - \theta_0)\sin e_\theta, \\
\alpha_{3x} &= -cz_{1R}\cos e_\theta\cos(\theta + \theta_0) \\
&\quad - cz_{2R}\cos(\theta - \theta_0)\cos e_\theta \\
&\quad - cz_{1R}\sin(\theta + \theta_0)\sin e_\theta \\
&\quad - cz_{2R}\sin(\theta - \theta_0)\sin e_\theta, \\
\alpha_{1y} &= c\sin(\theta_R + \theta_0)\cos e_\theta + c\cos(\theta_R + \theta_0)\sin e_\theta, \\
\alpha_{2y} &= c\sin(\theta_R - \theta_0)\cos e_\theta + c\cos(\theta_R - \theta_0)\sin e_\theta, \\
\alpha_{3y} &= -cz_{1R}\sin(\theta + \theta_0)\cos e_\theta \\
&\quad - cz_{2R}\sin(\theta - \theta_0)\cos e_\theta \\
&\quad + cz_{1R}\cos(\theta + \theta_0)\sin e_\theta \\
&\quad + cz_{2R}\cos(\theta - \theta_0)\sin e_\theta
\end{aligned}$$

where $\cos\theta_0 = R/\sqrt{R^{2+d^2}}$, $\sin\theta_0 = d/\sqrt{R^{2+d^2}}$ is nonzero except for $\theta_0 = 0$. A 6 m × 8 m workspace was set as the experimental environment for the considered robot, whose system parameters are listed in Table 4. The proposed CCPP was verified in two conditions—"no obstacles" and "with fixed and moving obstacles" within the workspace. The flowchart of the verification is illustrated in Fig. 12, in which the via points were computed by using the optimal CCPP in Section 3. These points were transmitted sequentially to BL2600 and then relayed to RCM4510 for the calculation of PWM motor control commands. The controller kept receiving the state information after the present-section navigation. The control system proceeded to the next tracking task if the tracking error has been within the tolerable range.

Fulfilling the whole tracking task by the flowchart in Fig. 12 brings the three results: 1) the power consumptions of the minimum time, minimum energy, and mixed modes in Tables 5, 6 and 7, respectively; 2) the real robot paths in the corresponding modes without/with fixed and moving obstacles in Figs. 13 and 14, respectively; and 3) the motor torques in Figs. 15, 16 and 17 when there were/won't obstacles. All of the coordinates in Figs. 13 and 14 are in Cartesian coordinates. Consider the obstacle settings of the workspace in Fig. 14. A moving object was initially

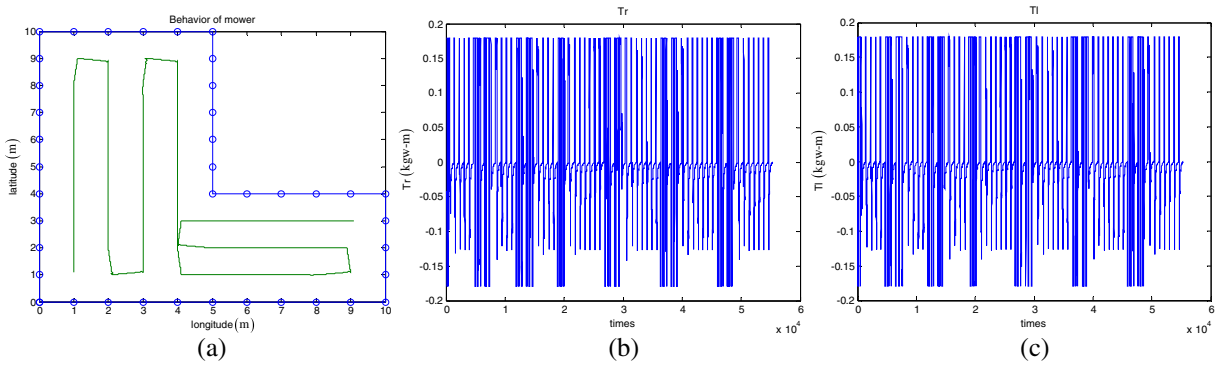

(a) (b) (c)

Fig. 18 Result of Mao et al. [30], **a** moving path, **b** right motor torque, **c** left motor torque

located at (173902.7, 2680451)(m) and moved toward (173906, 2680457.6)(m) under the speed 1.1 (m/s), estimated by the strategy in Section 3.2; its moving trajectory is described by the diagonal line in Fig. 14 while there were three fixed obstacles at (173904.6, 2680457.2)(m), (173901.9, 2680455)(m), and (173902.9, 2680453)(m), respectively. From Figs. 13–17, it can be obvious that the tracking task was completed by using the proposed controller guaranteeing -0.18 kg-m $\leq \tau_r$, $\tau_l \leq 0.18$ kg-m.

After the verification of the feasibility of our CCPP, a comparison between the CCPPs of this paper and [30] within the workspace of Fig. 10 in [30] was conducted to address the efficiency of our method. Two kinds of paths—the optimal path in the mixed mode and that in Fig. 10 of [30]—were considered in the comparison; the optimal route was proposed by substituting the parameter settings in Table 8 into Eq. 9. Performing trajectory tracking for these two paths brings the experimental results in Figs. 18 and 19 by applying the same controller (Eq. 26) in the previous verification. Verification and comparison are elaborated next.

5.4 Comparison of Working Time and Energy Consumption

The power consumptions in Tables 5–7 show that the consumed power for the minimum energy or minimum time mode is smaller/larger than those of other modes. This is consistent with the analysis of Eq. 2 and implies that: 1) tracking the path with the minimal k would consume less energy than those of other modes under the same time consumption, and 2) tracking the route with the maximal k may achieve less time cost than those of other modes under the same energy consumption.

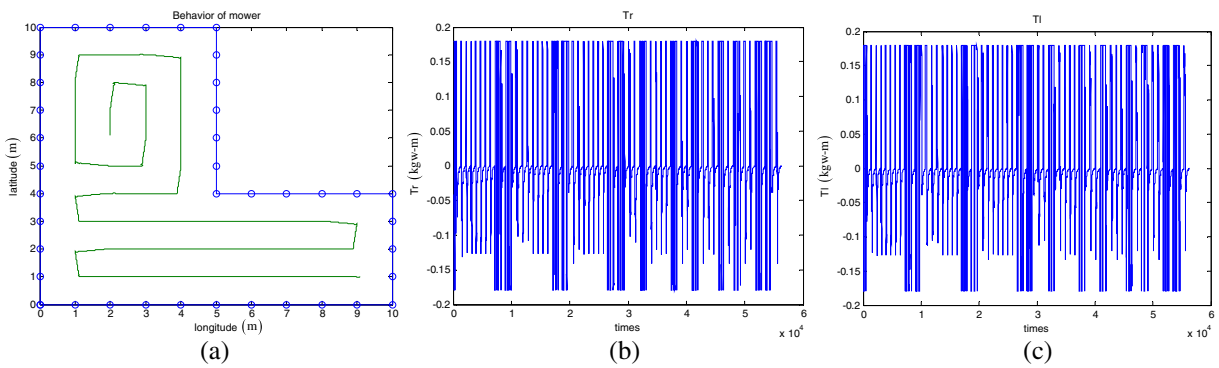

(a) (b) (c)

Fig. 19 Results of our work, **a** moving path, **b** right motor torque, **c** left motor torque

5.5 Indices of Dangerousness and Difficulty

In Fig. 13, it can be observed that the CCPP combined with the difficulty index yields the path featuring high tracking task easiness; therefore, the optimal path was smoothed and shortened in a systematic and efficient way. Moreover, the results in Fig. 14 imply that applying the dangerousness index in CCPP offers the function of avoiding the fixed or moving objects. This confirms that our obstacle avoidance strategy is able to assure human safety if there are living objects within the working field.

5.6 Results of Comparison

Figures 18 and 19 display the robot trajectories of tracking the path in the mixed mode with the time cost 576 s and that in Fig. 10 of [30] with the time consumption 594 s, respectively. Obviously, ours saved 18 s than that of [30]. This reveals superiority of the present approach.

6 Conclusion

This paper has studied the optimal CCPP for a mobile robot with the capability of offering minimum working time, minimum energy consumption, and mixed operation modes. Also, obstacle avoidance for fixed or moving objects is proposed in the CCPP by using two indices—a difficulty index implemented to ensure easiness of the obstacle avoidance and a dangerousness index possessing the advantage of avoiding either the static or dynamic obstacles in the working field. Human safety is simultaneously guaranteed by adopting the dangerousness index to establish the avoiding strategy. After the CCPP featuring the cost minimization and high human safety, a backstepping controller is proposed to enable the robot to track the optimal route. Verification of the proposed CCPP and a comparison between a published CCPP and ours were conducted to approve our superiority in the implementation of the mobile robot with a differential drive. The verification results indicate that the proposed planner contributed a benefit of minimizing the time or energy consumption with the obstacle avoidance.

Extension of the presented results to deal with the CCCP problem with a group of collaborative mobile robots is worthy of further study and is currently under development.

References

1. Choset, H.: Coverage for robotics-a survey of recent results. Ann. Math. Artif. Intell. **31**, 113–126 (2001)
2. Zu, L., Wang, H., Yue, F.: Localization for robot mowers covering unmarked operational area. In: Proc. IEEE/RSJ Int. Conf. Intelligent Robots and Syst., pp. 2197–2202 (2004)
3. Lee, T.K., Baek, S.H., Oh, S.Y., Choi, Y.H.: Complete coverage algorithm based on linked smooth spiral paths for mobile robots. In: Proc. Int. Conf. Control, Automation, Robotics and Vision, pp. 609–614 (2010)
4. Yang, S.X., Luo, C.: A neural network approach to complete coverage path planning. IEEE Trans. Syst. Man Cybern. **34**(1), 718–725 (2004)
5. Luo, C., Yang, S.X., Stacey, D.A., Jofriet, J.C.: A solution to vicinity problem of obstacles in complete coverage path planning. In: Proc. IEEE Int. Conf. Robotics and Automation, pp. 612–617 (2002)
6. Qiu, X., Song, J., Zhang, X., Liu, S.: A complete coverage path planning method for mobile robot in uncertain environments. In: Proc. World Congress on Intelligent Control and Automation, pp. 8892–8896 (2006)
7. Qiu, X., Liu, S., Yang, S.X.: A rolling method for complete coverage path planning in uncertain environments. In: Proc. IEEE Int. Conf. Robotics and Biomimetics, pp. 146–151 (2004)
8. Luo, C., Yang, S.X., Stacey, D.A.: Real-time path planning with deadlock avoidance of multiple cleaning robots. In: Proc. IEEE Int. Conf. Robotics and Automation, pp. 4080–4085 (2003)
9. Sipahioglu, A., Kirlik, G., Parlaktuna, O., Yazici, A.: Energy constrained multi-robot sensor-based coverage path planning using capacitated arc routing approach. Robot. Auton. Syst. **58**, 529–538 (2010)
10. Yao, Z.: Finding efficient robot path for the complete coverage of a known space. In: Proc. IEEE/RSJ Int. Conf. Intelligent Robots and Systems, pp. 3369–3374 (2006)
11. Jimenez, P.A., Shirnzadeh, B., Nicholson, A., Alici, G.: Optimal area covering using genetic algorithms. In: Proc. IEEE/ASME Int. Conf. Advanced Intelligent Mechatronics, pp. 1–5 (2007)
12. Wang, M., Tan, S., Yan, L.: Complete coverage path planning of wall-cleaning robot using visual sensor. In: Proc. Int. Conf. Electronic Measurement and Instruments, pp. 159–164 (2007)
13. Zhang, G., Ferrari, S., Qian, M.: An information roadmap method for robotic sensor path planning. J. Intell. Robot. Syst. **56**(1–2), 69–98 (2009)
14. Liu, Y., Lin, X., Zhu, S.: Combined coverage path planning for autonomous cleaning robots in unstructured

environments. In: Proc. World Congress on Intelligent Control and Autom., pp. 8271–8276 (2008)
15. De Carvalho, R.N., Vidal, H.A., Vieira, P., Ribeiro, M.I.: Complete coverage path planning and guidance for cleaning robots. In: Proc. IEEE Int. Sym. Industrial Electronics, pp. 677–682 (1997)
16. Liu, S., Sun, D., Zhu, C.: Coordinated motion planning for multiple mobile robots along designed paths with formation requirement. IEEE/ASME Trans. Mechatron. **16**(6), 1021–1032 (2011)
17. Mao, Y., Dou, L., Chen, J., Fang, H., Zhang, H., Cao, H.: Combined complete coverage path planning for autonomous mobile robot in indoor environment. In: Proc. Asian Control Conf., pp. 1468–1473 (2009)
18. Luo, C., Yang, S.X.: A bioinspired neural network for real-time concurrent map building and complete coverage robot navigation in unknown environments. IEEE Trans. Neural Netw. **19**(7), 1279–1298 (2008)
19. Oh, J.S., Choi, Y.H., Park, J.B., Zheng, Y.F.: Complete coverage navigation of cleaning robots using triangular-cell-based map. IEEE Trans. Ind. Electron. **51**(3), 718–726 (2004)
20. Garcia, E., Gonzalez de Santos, P.: Mobile-robot navigation with complete coverage of unstructured environments. Robot. Auton. Syst. **46**, 195–204 (2004)
21. Shair, S., Chandler, J.H., Gonz'alez-Villela, V.J., Parkin, R.M., Jackson, M.R.: The use of aerial images and GPS for mobile robot waypoint navigation. IEEE/ASME Trans. Mechatron. **13**(6), 692–699 (2008)
22. Chwa, D.: Tracking control of differential-drive wheeled mobile robots using a backstepping-like feedback linearization. IEEE Trans. Syst. Man Cybern. Part A Syst. Hum. **40**(6), 1285–1295 (2010)
23. Park, B.S., Yoo, S.J., Park, J.B., Choi, Y.H.: A simple adaptive control approach for trajectory tracking of electrically driven nonholonomic mobile robots. IEEE Trans. Control Syst. Technol. **18**(5), 1199–1206 (2010)
24. Yavuz, H., Bradshaw, A.: A new conceptual approach to the design of hybrid control architecture for autonomous mobile robots. J. Intell. Robot. Syst. **34**(1), 1–26 (2002)
25. Shiu, B.M., Lin, C.L.: Design of an autonomous lawn mower with optimal route planning. In: Proc. IEEE Int. Conf. Industrial Technology, pp. 1–6 (2008)
26. Hsu, P.M., Lin, C.L.: Optimal planner for lawn mowers. In: Proc. IEEE Int. Conf. Cybernetics Intelligent Syst., pp. 1–7 (2010)
27. Sisbot, E.A., Marin-Urias, L.F., Alami, R., Simeon, T.: A human aware mobile robot motion planner. IEEE Trans. Robot. **23**(5), 874–883 (2007)
28. Yamamoto, Y., Yun, X.: Coordinating locomotion and manipulation of a mobile manipulator. IEEE Trans. Autom. Control **39**(6), 1326–1332 (1994)
29. Do, K.D., Jiang, Z.P., Pan, J.: Simultaneous tracking and stabilization of mobile robots: an adaptive approach. IEEE Trans. Autom. Control **49**(7), 1147–1152 (2004)
30. Mao, Y., Dou, L., Chen, J., Fang, H., Zhang, H., Cao, H.: Combined complete coverage path planning for autonomous mobile robot in indoor environment. In: Proc. Asian Control Conf., pp. 1468–1473 (2009)